



HAL
open science

Modeling the Impact of Seasonal Water Table Fluctuations on Ambient Noise Interferometry Using Acousto-Elastic Effect

Yunliang Wang, Jean Schmittbuhl, Jerome Azzola, Flavien Mattern, Dimitri Zigone, Olivier Lengliné, Vincent Magnenet, Jérôme Vergne

► **To cite this version:**

Yunliang Wang, Jean Schmittbuhl, Jerome Azzola, Flavien Mattern, Dimitri Zigone, et al.. Modeling the Impact of Seasonal Water Table Fluctuations on Ambient Noise Interferometry Using Acousto-Elastic Effect. *Geophysical Research Letters*, 2024, 51 (18), pp.e2024GL110239. 10.1029/2024GL110239 . hal-04704511

HAL Id: hal-04704511

<https://hal.science/hal-04704511v1>

Submitted on 23 Sep 2024

HAL is a multi-disciplinary open access archive for the deposit and dissemination of scientific research documents, whether they are published or not. The documents may come from teaching and research institutions in France or abroad, or from public or private research centers.

L'archive ouverte pluridisciplinaire **HAL**, est destinée au dépôt et à la diffusion de documents scientifiques de niveau recherche, publiés ou non, émanant des établissements d'enseignement et de recherche français ou étrangers, des laboratoires publics ou privés.



Distributed under a Creative Commons Attribution - NonCommercial - NoDerivatives 4.0 International License

Geophysical Research Letters®










RESEARCH LETTER

10.1029/2024GL110239

Modeling the Impact of Seasonal Water Table Fluctuations on Ambient Noise Interferometry Using Acousto-Elastic Effect

Key Points:

- We develop an acousto-elastic model for seismic wave scattering in a deforming layered subsurface
- Stress fluctuations induced by seasonal water table variations are shown to be responsible for significant changes in seismic velocities
- The model is providing an interpretation tool for environmental monitoring signals obtained from ambient seismic noise

Y. Wang¹ , J. Schmittbuhl¹ , J. Azzola^{1,2}, F. Mattern¹ , D. Zigone¹ , O. Lengliné¹ , V. Magnenet³ , and J. Vergne¹ 

¹ITES UMR 7063, Université de Strasbourg/CNRS, Strasbourg, France, ²Karlsruhe Institute of Technology (KIT), Institute of Applied Geosciences (AGW), Karlsruhe, Germany, ³ICube UMR 7357, Université de Strasbourg/CNRS, Strasbourg, France

Supporting Information:

Supporting Information may be found in the online version of this article.

Correspondence to:

J. Schmittbuhl,
Jean.Schmittbuhl@unistra.fr

Citation:

Wang, Y., Schmittbuhl, J., Azzola, J., Mattern, F., Zigone, D., Lengliné, O., et al. (2024). Modeling the impact of seasonal water table fluctuations on ambient noise interferometry using acousto-elastic effect. *Geophysical Research Letters*, 51, e2024GL110239. <https://doi.org/10.1029/2024GL110239>

Received 11 MAY 2024
Accepted 28 AUG 2024

Abstract Ambient noise interferometry has become a common technique for monitoring slight changes in seismic velocity in a variety of contexts. However, the physical origin of the resolved small velocity fluctuations is not well established for long-term seasonal effects. Here we propose a physical forward model of scattered waves in a deformable medium that includes acousto-elastic effect, which refers to non-linear elasticity with third-order elastic constants. The model shows that small pressure perturbations of a few kPa due to seasonal variations in the water table can induce seismic velocity changes compatible with those measured at the surface by ambient noise interferometry. The results are consistent with field observations near the deep geothermal site of Rittershoffen (France). They illustrate the capability in modeling the diffuse wavefield from scattering synthetic waves to reproduce ambient noise signals for monitoring environmental and/or deep reservoir signals.

Plain Language Summary Monitoring the fine evolution of the Earth's crust either prior to catastrophic events such as earthquakes or landslides, or georesource exploitation, is an important objective for risk management. Ambient noise interferometry is one of the emerging tools for assessing the minute evolution of seismic velocities in the subsurface. However, the physical origin of the observed small velocity changes is not well established. Here we propose a physical model of scattered waves in a deformable medium that includes non-linear elastic effects, which are not conventionally considered. The model shows that small pressure perturbations of a few kPa due to seasonal variations in the water table can induce seismic velocity changes compatible with those measured at the surface by ambient noise interferometry. The results are consistent with field observations near the deep geothermal site of Rittershoffen (France). They illustrate the capability in modeling scattered synthetic waves to reproduce ambient noise signals.

1. Introduction

The use of Ambient Noise Interferometry (ANI) to continuously monitor environmental perturbations, including minute changes related to tides (Yamamura et al., 2003), atmospheric pressure (Silver et al., 2007), rainfall, atmospheric temperature (Hillers et al., 2015), snowfall (Mordret et al., 2016), or landslides (Mainsant et al., 2012), volcanoes (Brennguier et al., 2011; Sens-Schönfelder et al., 2014), fault zones (Brennguier et al., 2008; Obermann et al., 2014), seasonal changes of the crust (Wang et al., 2017) or deep geothermal reservoirs (Lehujeur et al., 2017; Sánchez-Pastor et al., 2019), is the subject of major development (e.g., Q. Y. Wang and Yao, 2020 for a review). This method is built upon cross-correlations of ambient seismic noise recorded at distinct seismic stations (see reviews of Campillo & Roux, 2015; Nakata et al., 2019). Ambient noise records from pairs of sensors are cross-correlated and the evolution of Ambient Noise Cross-Correlation Functions (ANCCFs) is analyzed over the monitoring period. Applied to the pervasive ambient noise, which is ubiquitous and permanent, it opens interesting perspectives for the continuous monitoring of environmental signals or processes induced at depth by geotechnical operations, such as the well pumping or injection of fluids (Obermann et al., 2015; Sánchez-Pastor et al., 2019).

When Green functions can be reconstructed from ANCCFs, time evolution of their codas (i.e., the late part of Green function) through Coda wave Interferometry (CWI) enable to infer slight changes in the medium over time (Brennguier et al., 2008; Campillo & Roux, 2015; Sens-Schönfelder et al., 2014). Indeed, CWI technique is based on the high sensitivity to slight medium perturbations of the scattered waves (Snieder, 2006). However, a clear

© 2024. The Author(s).

This is an open access article under the terms of the [Creative Commons Attribution-NonCommercial-NoDerivs License](https://creativecommons.org/licenses/by-nc-nd/4.0/), which permits use and distribution in any medium, provided the original work is properly cited, the use is non-commercial and no modifications or adaptations are made.

connection of the observed changes of coda waves with the physical processes undergoing at depth in the subsurface, is still questionable (Sens-Schönfelder & Wegler, 2006; Yates et al., 2019; Zhan et al., 2013). A better understanding of the ANI measurements is thus necessary for the interpretation of the evolution of ANCCFs, in particular in terms of subsurface deformation, and is a necessary step to the application of such methods to the monitoring of underground structures with a depth of several kilometers in order to remove near-surface effects that might be dominant in the observed signal.

Along this perspective, Azzola et al. (2018, 2020) demonstrated experimentally and numerically the sensitivity of the diffused wavefield to volumetric and reversible deformation at laboratory scale due to non-linear acousto-elastic effect. The acousto-elastic effect refers to velocity changes of waves propagating through an elastic material when subjected to a static stress field (Hughes & Kelly, 1953). Accordingly, changes in elastic wave velocities during stress-induced deformation can result from acousto-elastic effects (Aoki, 2015). The phenomenon has been theoretically explained by considering a higher order in the expression of the elastic energy, which implies introducing non-linear relationships between stresses and strains (Smith, 1963). Indeed, the stored elastic energy per unit of undeformed volume, noted W_{elas} , can then be expressed as a function of the components of the strain tensor ϵ :

$$W_{elas}(\epsilon) = \frac{1}{2} \cdot C_{ijkl}^{(2)} \cdot \epsilon_{ij} \cdot \epsilon_{kl} + \frac{1}{6} \cdot C_{ijklmn}^{(3)} \cdot \epsilon_{ij} \cdot \epsilon_{kl} \cdot \epsilon_{mn} + \dots \quad (1)$$

Equation 1 uses an implicit summation, following Einstein's convention. The coefficients $C_{ijkl}^{(2)}$ refer to the second-order elastic constants, that is, the Lamé's coefficients when the solid is isotropic. The coefficients $C_{ijklmn}^{(3)}$ are the third-order elastic constants (TOECs) related to the Murnaghan constants: L , M and N (Smith, 1963; Toupin & Bernstein, 1961). When strain is small, only the first term, involving the second-order elastic constants, is retained in the sum of Equation 1. The resulting expression describes a first order approximation of the stored elastic energy. When strain is larger, a higher expansion of the stored energy has to be considered, and third-order elastic constants need to be taken into account. Based on this formalism, Hughes and Kelly (1953) showed that the velocities of the compression and shear waves vary by an amount which is proportional to the load, even for an isotropic elastic material. Furthermore, the acousto-elastic theory predicts that the elastic deformation of the medium causes the propagation of an anisotropic wavefield whose wave velocities depend on the strain field. This anisotropic behavior results from non-linearities in the stress-strain relationship.

Hughes and Kelly (1953) related the strain tensor to the current and initial stress tensors using pseudo second-order elastic coefficients C_{ijkl}^* :

$$\sigma_{ij} = \sigma_{ij}^0 + \sum_{kl} C_{ijkl}^* \epsilon_{kl}, \quad (2)$$

where the coefficients C_{ijkl}^* depend notably on the components of the strain tensor ϵ and the third-order elastic parameters (L , M and N) (Azzola et al., 2020). The influence of the strain tensor implies non-linear relations between stresses and strains. Following Equation 2, the elastic response of the material causes the propagation of an anisotropic wavefield whose wave velocities depend, in each direction, on the current state of deformation of the medium. Using such a formalism, Azzola et al. (2020) showed that acousto-elastic effects play a major role in the influence of elastic strain on CWI.

Our objective in this study is to propose a physical link between small deformation (of the order of 10^{-6}) in the subsurface from stress changes at the ground surface (of the order of 10 kPa) resulting from seasonal metric water table elevation changes, and relative seismic wave velocity changes (of the order of 10^{-3}) measured using ANCCFs. For this, we introduce a numerical forward model for scattered waves in a deformable medium that includes acousto-elastic effect following the approach of Azzola et al. (2018, 2020). We model the subsurface deformation from stress changes applied at the ground surface (of the order of 10 kPa). We assume in our study that stress changes are induced only by the weight fluctuations of the subsurface aquifer and not by poro-elastic effects in the bulk. Other studies have compared both effects on the seismic velocities (e.g., Tsai, 2011). To test the model, we compare the numerical predictions with field observations of the long-term (9 year) evolution of ANCCFs computed from a pair of seismic stations close to the geothermal site of Rittershoffen (Rhine Graben, France) where water table elevation was monitored over the same period. This test has the limitation of using a single pair of seismic stations, which may emphasize various biases of ANCCF measurements resulting from

uneven distribution of the wave sources or azimuthal directional bias that exists in the area (Lehuteur et al., 2015) but allows for a fine comparison between observations and simulations. A regional study using a large set of stations to assess spatial distribution of the ANCCF variations will be addressed in a forthcoming work.

Section 2 presents the field observations of the seasonal effects in the ANCCFs at the Rittershoffen site and their correlation with the local water table changes. The principle of the 2D numerical model is described in Section 3. The model is 12 km in lateral extension to largely cover the distance between the pair of stations. It combines a physical domain that is 4 km deep, made of physical layers that models the upper part of the Rhine Graben and a virtual domain that is 16 km deep, located below, where scattered waves are produced from a point source. In both domains, we compute quasi-static deformation induced by stress changes applied at the surface of the model. An important specificity of our modeling approach is to take into account acousto-elastic effect owed to non-linear elasticity. Wave propagation is performed iteratively taking into account the deformed medium. In Section 4, we show the good match between the results of the model and the field observations that explain the origin of the velocity changes evidenced in the first hundred meters of the subsurface.

2. Field Measurements

2.1. Data and Processing

In this study, we focus on the geothermal Rittershoffen project (France), located seven km to the southeast of the historical pilot plant of Soultz-sous-Forêts. It consists of a doublet of wells drilled during fall 2012 for the first one (GRT1) and spring 2014 for the second one (GRT2). The wells reach a depth of 2526 and 2708 m (TVD) respectively and cross an en-echelon normal fault zone at depth (Baujard et al., 2017; Lengliné et al., 2017). We used data from the permanent seismic network that has been deployed around the site between 2012 and 2021. During that period, the network was composed of four stations equipped with three-components short period 1 Hz sensors (L4C 3D) and digitized by Quanterra Q330S at 100 Hz or 200 Hz. Here we focus on two of these stations (RITT and BETS stations), which are 2.6 km apart and located in the vicinity of the geothermal power plant, respectively 1.6 km to the east and 1.0 km to the west of the platform (Figures 1a and 1b). We also take advantage of the well logging information that constrain the seismic velocity model below the station pair.

A spectral analysis of the continuous records was performed to estimate the various sources of ambient noise in the area (Lehuteur et al., 2015). As classically observed, the spectrograms show a clear change in the noise pattern at ~ 1 Hz (Figure S1 in Supporting Information S1). At lower frequencies, the dominant sources of noise correspond to the microseismic peak originating from the interaction between ocean swells and sea floor in the North Atlantic Ocean, exhibiting a clear annual periodicity with stronger amplitudes during winter periods. At frequencies higher than 1 Hz, weekly and diurnal periodicities typical of anthropogenic sources due to human activities in the villages and traffic along nearby roads, are observed (Lehuteur et al. (2015, 2017)).

The preprocessing of the continuous records at the RITT and BETS stations includes the sequencing in 1 day long records, a down sampling at 10 sps, a spectral whitening (by replacing the amplitude spectrum with a step window between 1 and 3 Hz). These modified 1 day records are cross-correlated to produce ANCCFs, which are then averaged over 10 days with a 10 day time step. Figure 1c shows the time evolution of the East-East (EE) component of the ANCCF calculated from the East components of the three-component (E, N, Z) RITT and BETS stations. The EE component of the ANCCFs was selected as it is the closest to the Radial-Radial (RR) component computed from the 2D numerical model oriented along the station pair azimuth. Polarity analysis of the observed ANCCF is shown in Figure S2 in Supporting Information S1. It shows that RR components are dominated by Rayleigh waves on the contrary to transverse-transverse (TT) components, which include slow Love waves.

2.2. Relative Time Delay in the 1–3 Hz Frequency Band

To assess the time evolution of the ANCCF, a stretching technique is applied to the whole signal to estimate the relative time delay ε as the factor by which the time axis of one of the traces must be stretched or compressed to obtain the best correlation with the other trace. In this technique, one defines a “stretched” version of the reference signal: $S(t) = R((1 + \varepsilon)t)$, given the coefficient of stretching ε (Sens-Schönfelder & Wegler, 2006). The time-series of the computed stretching coefficient (dt/t) for the causal and acausal parts of ANCCFs are shown in Figure S3 in Supporting Information S1. The variations of dt/t from both parts of ANCCF, are in good agreement

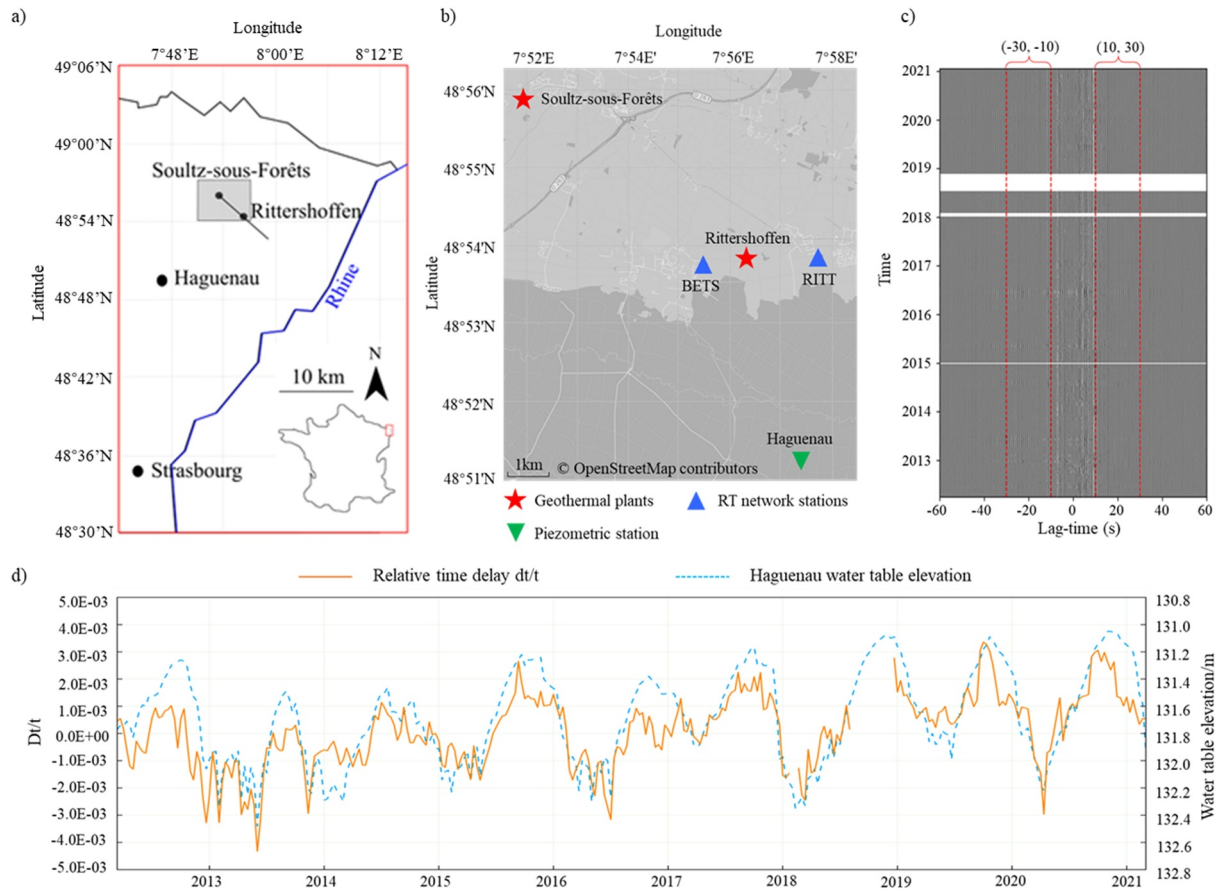


Figure 1. (a) Regional map locating the geothermal fields of Rittershoffen and Soultz-sous-Forêts and the studied area (gray box) in the east part of France; (b) Zoom on the studied area: location of the BETS and RITT seismic stations, and the Haguenau piezometric station using a OpenStreetMap background image; (c) Ambient noise cross-correlation functions (ANCCF) using East components of stations RITT and BETS, averaged over 10 days and filtered between 1 and 3 Hz; Each line is a gray coded representation of the ANCCF for a lag time between -60 and $+60$ s, the red dotted vertical lines represent time windows (-10 to -30 s and 10 – 30 s) used to compute relative time delay with stretching method. White zones correspond to periods of lack of data; (d) comparison of temporal variation of the subsurface water table elevation (in meters with respect to sea level) measured at the Haguenau forest station for 9 years and relative time delay dt/t estimated from stretching of ANCCFs using the [10–30 s] time window.

not only in amplitudes of dt/t but also along the time evolution. Indeed, the correlation coefficient between causal and acausal dt/t evolution, is high (0.94). The difference between these two parts (Figure 1c) may be caused by the uneven distribution of the seismic noise (Lehuteur et al., 2015) or interstation distances limitation (Luo et al., 2015). To further mitigate possible bias, we compute the stretching coefficients after averaging the causal and acausal parts of ANCCFs, following the methods outlined by Paul et al. (2005), Sabra et al. (2005), Brenguier et al. (2020) and Mordret et al. (2020). We take advantage of the long and almost uninterrupted time series (gaps in 2018 are due to temporary acquisition issues) to study the applicability of monitoring approaches based on the ANCCF. Indeed, such technique have already demonstrated their ability to highlight minute relative time delay from the related variations of ANCCF computed from ambient noise recorded at pair of stations (Lehuteur et al., 2017). In the 1–3 Hz frequency band, we observe a high mean coherence value of the ANCCF for most of the period. Both the phase and the relative amplitudes of these relative time delays show strong seasonal effects (Figure 1d).

2.3. Water Table Elevation

In Figure 1d, we compare the evolution of the observed stretching coefficient ε with the daily measures of the local variations of the water table elevation. These hydrogeological data are obtained from the piezometric station closest to the seismic stations and recording data over the same study period. The station, which is located 5 km south of the Rittershoffen geothermal site, in the Haguenau forest, is part of the regional network APRONA

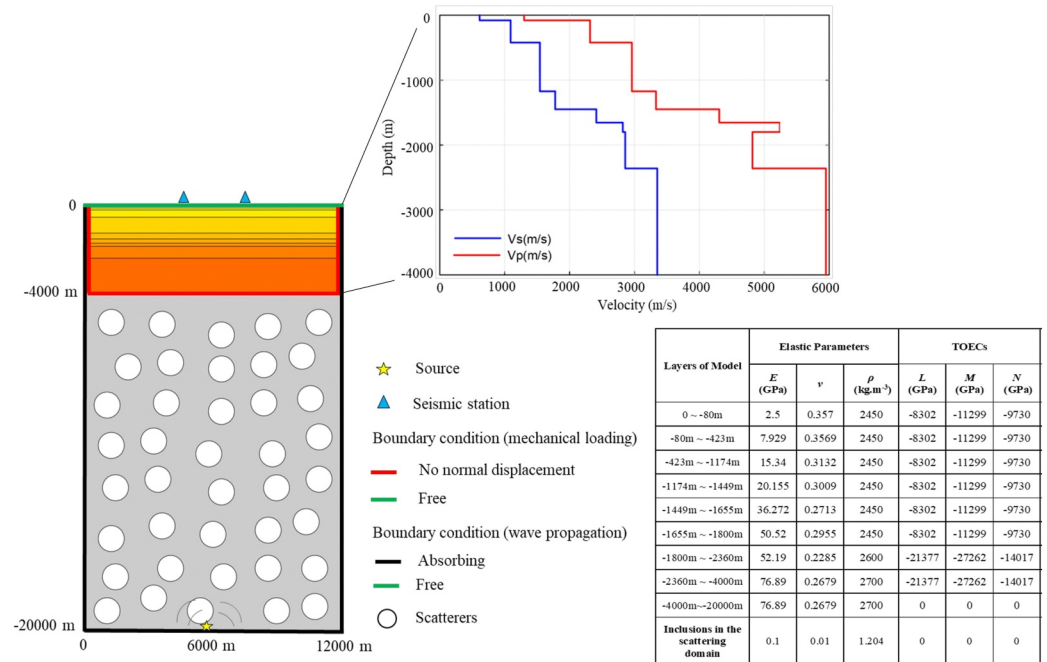


Figure 2. (left panel) Sketch of the 2-D numerical model and its boundary conditions used during the simulation of wave propagation and elastic deformation. It includes a top domain with a multi-layered representation (8 layers) of the 4 first km of the Rittershoffen subsurface. Below is a sub-model (16 km in depth), that consists in a virtual scattering domain (gray background) with round inclusions of 1.8 km diameter (white circles) that behave as wave scatters (top panel) Vp and Vs velocity model with 8 layers deduced from the sonic log measured along the GRT-1 well at Rittershoffen site (Maurer et al., 2020). (right panel) Table of elastic parameters and third-order elastic constants (TOECs) used in Code_ASTER and Specfem2D for the numerical model from Vallier et al. (2018) and Winkler and Liu (1996).

(station 01995X0103/338B1). As shown in Figure 1d, the water table fluctuations are clearly correlated to the stretching coefficient evolution, the correlation coefficient is around 0.93. Such observations have been obtained in other contexts (Gaubert-Bastide et al., 2022; Voisin et al., 2016).

An open question is how to explain the signature on the stretching coefficient (or related wave velocity change) of such a small stress or strain perturbation. Indeed, they are of the order of 2 m, which represent very small pressure fluctuations on the top of the reservoir, of the order of 0.02 MPa. With such a stress perturbation, the related elastic strain is of the order of $1.3 \cdot 10^{-6}$ using a representative Young modulus of 15 GPa (Vallier et al., 2019), and the stretching coefficient of the same order of magnitude (Azzola et al., 2018). This means that the water-table induced velocity variations must be explained by another mechanism. Moreover, if this mechanism is well established, it will become possible to remove it and open the perspective to detect smaller velocity variations related to deeper structures.

3. Modeling of Wave Scattering During Acousto-Elastic Deformation

3.1. Description of the Model

To better understand the process at the origin of these measurements, we followed the numerical approach developed by Azzola et al. (2018, 2020). The approach aims at modeling the variations of the relative time delay ϵ estimated from the RITT and BETS records. The numerical model is a 2D model separated in two parts: a physical representation of the subsurface on top of a virtual domain where scattered waves are produced (Figure 2). The top part of the model represents a geological section of the subsurface in the vicinity of the Rittershoffen site. It is made of height layers that represent the various sedimentary layers and the thick granitic basement, following the sonic log and vertical seismic profiles (VSPs) measured in the RITTER1 well at the Ritterhoffen site (Maurer et al., 2020) (Figure 2). The lower part of the model includes numerous virtual large circular scatterers that have a strong impedance contrast with the bulk. They intend to strongly scatter the wavefield emitted from a point source at the bottom of the model with a Ricker function peaked at 2 Hz. This virtual section of the model aims at

producing wave scattering properties similar to those measured from recorded ambient noise. In doing so, we assume that the sedimentary layers in the upper part of the model are homogeneous at the scale of the scatters (1.8 km in diameters).

To model the impact of the variations of the water table elevation, we converted the water table elevation measurements into relative pressure variations using a water density of $1,000 \text{ kg m}^{-3}$. We applied the computed pressure perturbations on the top boundary of the numerical model, taking the water table elevation observed at the beginning of the time-series as a reference. The stress loading applied at the top of the model to reproduce the observed water table changes, acts mechanically through the whole sample. The induced elastic deformation is obtained using a finite element method (Code_ASTER). Wave propagation is simulated in the iteratively deformed mesh using a spectral element approach (SPECFEM2D). The modeling approach implements the effect of acousto-elasticity, as proposed by Azzola et al. (2018, 2020). Pseudo second-order elastic coefficients C^*_{ijkl} are computed while the medium is progressively deformed. The coefficients are computed for each spectral element of the mesh grid in SPECFEM2D from the quasi-static deformation field. The latter is calculated at each node of the model using Code_ASTER, considering the second order approximation of the elastic energy W_{elas} which includes only the second-order elastic constants, that is, the Lamé's coefficients.

For the boundary conditions (Figure 2), the bottom as well as the right and left boundaries are set as absorbing in the wave propagation simulation. The absorbing boundary condition is a so-called Stacey boundary condition (Stacey, 1988). Along the interface between the subsurface model and the scattering sub-model, we preserve continuity in stresses and displacements. The scattered wavefield illuminates the system persistently over the duration of recording, that is, 40 seconds. The top of the model has free boundary condition where the pair of seismic stations is set with the same inter-distance of 2.6 km as in the field (Figure 2). The synthetic ANCCFs are built from transmitted scattered waves at this pair of virtual seismic stations.

Our numerical model describes the reservoir as composed of homogeneous and isotropic units and does not depict in detail the complexity of each geological layer. We use information from the nearby Soultz-sous-Forêts site to characterize the properties of the geological units (see Figure 1). Vallier et al. (2018) present a synthesis of the relevant rock properties obtained either from laboratory measurements on cored samples or from geophysical investigations. Young's modulus E , Poisson ratio ν and density ρ are defined for the sedimentary layers and for the lower granitic domain are given Figure 2 (Vallier et al., 2018; Winkler & Liu, 1996). The TOECs are chosen from Winkler and Liu (1996) who inverted the TOECs for a variety of rock samples under uniaxial and hydrostatic stress conditions. No acousto-elastic effects are introduced in the virtual scattering domain where TOECs are set to zero.

3.2. Validation of the Model

For a validation of the approach, we compare the scattering properties deduced from the ambient noise recorded at RITT and BETS pair of stations in the vicinity of Rittershoffen, to those computed from the numerical model. We base our comparison on the measure of the temporal variation of the dimensionless seismic energy $U(r,t)$ and on the estimation of the mean free path from a least squares regression comparing the measurement to a simple diffusion model (Azzola et al., 2018; Olivier et al., 2015; Wegler & Lühr, 2001). Figure S4 in Supporting Information S1 shows the evolution of $\ln(U(t))$, calculated from simulated and field measurements, using the 30 s long causal and acausal parts of the ANCCFs. It evidences the progressive stabilization of the seismic energy which is characteristic of the diffusion regime. It shows that the numerical model reproduces well the scattering behavior of the geological domain sampled by the ANCCFs. Figure S4 in Supporting Information S1 also represents the best fit of the energy function assuming a diffusion model. From this fit, we deduce the mean free path $l = 2.11 \text{ km}$ in the numerical case and $l = 2.21 \text{ km}$ with the measurements at the RITT and BETS stations. The agreement between the estimated mean free paths also indicates that the numerical model reproduces the wave scattering in the subsurface.

3.3. Predicted Relationship Between Water Table Variation and Relative Time Delays Dt/t

To predict the evolution of dt/t induced by the pressure changes induced by water table variation, we computed the relationship between the applied pressure σ at the surface and the induced stretching coefficient, $\varepsilon = dt/t$ for the velocity model described in Figure 2. We assume a constant time window [10–30 s] for stretching coefficient

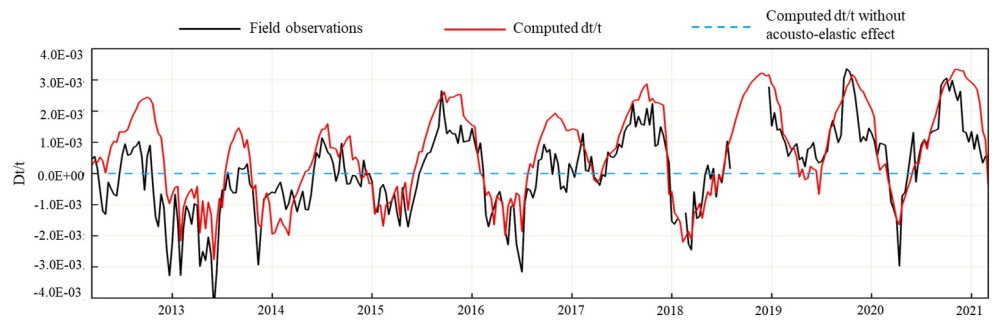


Figure 3. Comparison of the time-series of the stretching coefficient $\epsilon = dt/t$ computed either from observed water table fluctuations and using our acousto-elastic model (red line), or from correlation of the seismic noise recorded at stations RITT and BETS (black line). The dashed blue line is obtained when no acousto-elastic effect is considered in the model. In the latter case, amplitudes range from $-6.85 \cdot 10^{-7}$ to $5.13 \cdot 10^{-7}$ and are not visible with the chosen scale of the y-axis of the figure (detailed variations are plotted in Figure S4 in Supporting Information S1).

measurements at different applied pressures. The obtained relationship is shown to be linear (see Figure S5 in Supporting Information S1):

$$\epsilon = -4.06 \cdot 10^{-7} \sigma + 5.39 \cdot 10^{-5}. \quad (3)$$

4. Prediction of the Model for Monitoring Environmental Signals

Based on the relationship Equation 3 and a series of pressure changes at the surface, estimated from the measurements of the water table variation, the model predicts of the evolution of relative time delay dt/t . Subsequently, the evolution of ϵ in time is computed for the sequence of pressure changes deduced from the time-series of the water level elevation measured over the 9 years (2012–2021) (Figure 1d—blue dashed line), taking as a reference, the elevation at the beginning of the time series (Figure 3, red curve). Figure 3 also reproduces for comparison (black curve), the evolution of the stretching coefficient ϵ obtained from the field observations of the ambient seismic noise at RITT and BETS stations (Figure 1d—orange solid line). The red curve that is the modeled evolution of ϵ from the water table evolution, clearly correlates over time with the field observation curve of ϵ (black curve), demonstrating the physical link proposed by the model. To check the preponderant impact of acoustoelastic effects, we did simulations omitting acoustoelastic effects in the wave propagation modeling (dashed blue line in Figure 3 and Figure S6 in Supporting Information S1). We observe in this case that the relative time delays computed numerically are four orders of magnitudes lower. This result shows the importance of the non-linear elastic behavior of the subsurface below the pair of seismic stations. It also illustrates the sensitivity of ANI to very fine elastic and reversible deformation.

The $\epsilon = dt/t$ of field observations and simulations in Figure 3 are both computed with the stretching method, in which the time window is a significant parameter. According to the theory of CWI, only the coda part of the seismic waves illuminates the medium multiple times and is sensitive to slight medium perturbations. Subsequently, the choice of time window in the ANCCF to capture the coda wave, is an important choice. To confirm the choice of the time window for computing ϵ , we did several tests. First, we computed the Green function of the numerical model by replacing one of the stations by a source (and removing the source at bottom) but keeping the same velocity model (as shown in Figure S9a in Supporting Information S1). In other words, all physical parameters of this modified model (Figure S9a in Supporting Information S1) are similar to that in Figure 2. Based on the obtained synthetic Green function (Figure S9a in Supporting Information S1), the coda part starts at around 8 s. Second, we analyzed the observed average East-East component of ANCCF (left panel of Figure S9b in Supporting Information S1) and average radial-radial component of synthetic ANCCF (left panel of Figure S9c in Supporting Information S1), both reproduced on the same figure in Figure S10 in Supporting Information S1 for comparison. The amplitudes of both ANCCFs decrease significantly after approximately 9 or 10 s. Third, we analyzed the polarity of the observed ANCCF (Figure S2 in Supporting Information S1). It shows that the surface waves mainly arrive before 10 s for ANCCF of East-East component (not for the North-North component where

late Love wave arrivals are clearly visible). Hence, we selected the time window [10–30 s] in the ANCCF to apply the stretching method over the studied period both for the observed and synthetic data sets.

The depth sensitivity of the ANCCF is also an important feature to take into account. Figure S7 in Supporting Information S1 shows the kernel sensitivity of Rayleigh waves for our model. It indicates that the sensitivity is high in the depth range of 0 to -1.5 km with a peak at about -0.5 km. The amplitude of strain changes induced by water table variations is peaks between 0 and -1 km below surface, as shown in Figure S8 in Supporting Information S1. This range of depth coincides with the zone of highest sensitivity of the kernel.

The velocity model we used (top panel of Figure 2) is obtained from sonic logs and VSP measurements at the Rittershoffen GRT-1 well (Maurer et al., 2020) that is located between the pair of stations (BETS-RITT, see Figure S11 in Supporting Information S1). However, another velocity model has been proposed in the study area. Indeed, Lehujeur et al. (2017) inverted a velocity model from a well-resolved group-dispersion curve at relatively high frequencies (up to 5 Hz) using data from two small arrays (ARIT and AKUL - green squares in the Figure S11 in Supporting Information S1) slightly offset to the North of the BETS-RITT station pair, and a double beam forming approach. The velocity model is reproduced in Figure S12 in Supporting Information S1. To test the relevance of this velocity model, we computed synthetic Green's function using this model and found a poorer agreement with observations than using the Maurer et al. (2020) model (see Figure S13 in Supporting Information S1: (a) synthetic Green's function and observed EE cross-correlation function using the Maurer et al. (2020) velocity model; (b) synthetic Green's function and observed EE cross-correlation function using the Lehujeur et al. (2017) velocity model). This comparison confirmed our choice of using the velocity model of Maurer et al. (2020) for our simulations.

Here, we focus on the impact of a quasi-static loading caused by variations in the water content of a free aquifer on ANI measurements. Fluid-driven processes such as squirt flows or dynamic poro-elastic effects could also contribute to seismic velocity changes (Fokker et al., 2021, 2023; Liu et al., 2020; Pride et al., 2004; Tsai, 2011). But the effects of most of these processes are expected to be less significant comparing to that of water table fluctuations at current frequency band (in the range 1–3 Hz) and at the investigated spatial scales. In the 0.1–0.5 Hz frequency band, we also observe annual periodicity of the seismic velocity variations. However, these variations are not in phase with the ones observed in the 1–3 Hz band and are therefore probably not related to changes in the water-table elevation.

Seasonal variations have already been observed and associated with rainfalls or varying groundwater content (Obermann et al., 2014; Sens-Schönfelder & Wegler, 2006), thermoelastic effects in the Earth crust caused by changes in atmospheric temperature (Hillers et al., 2015), or with evolving ambient noise sources (Hillers & Ben-Zion, 2011). Seasonal signals are not only likely to be a product of multiple environmental processes contributing to the signal to different degrees, but they are also dependent on the regional setting and on the location of the study site (Wang et al., 2017). Therefore, the interpretation of the pluri-annual signals is site-sensitive. As an illustration, our conclusions differ from the ones drawn by Hillers et al. (2015), who observed seasonal variations in the arid area of the San Jacinto fault, using 6 years long of ambient seismic noise data. They investigated several source mechanisms likely to produce the seasonal fluctuations highlighted in the 0.5–2 Hz frequency band, with peak-to-peak changes up to 0.2%. Thermoelastic strain induced by changes in surface temperature were the dominant source mechanism. The other environmental effects investigated by Hillers et al. (2015), including rainfall, were found to contribute less significantly to the signal than thermoelastic effects. We also quantified the relative contribution to the signal of thermoelastic strain due to annual changes in surface temperature based on the numerical model in Figure 2, showing that the dt/t can reproduce seasonal changes due to atmospheric temperature variation, but the amplitudes of dt/t ($\sim 10^{-5}$) are lower than that induced by water table elevation ($\sim 10^{-3}$) by two orders (see Text S1 in Supporting Information S1 and Figure S14 in Supporting Information S1). Also, ambient noise is dominated in the 1–3 Hz frequency band, by a highly periodic anthropogenic noise (Lehujeur et al., 2015). Therefore, we excluded changes in noise sources to be at the origin of the seasonality and retained changes in the elevation of the groundwater table near Rittershoffen as the most likely source of the seasonal signal, noting moreover that the Rhine groundwater table is one of the most important in France and Europe (Thierion et al., 2012). The groundwater near Rittershoffen region belongs to one of Europe's major groundwater resources, namely Alsace aquifer system, the pressure head variations of which are related to infiltration of surface water in Vosges rivers and Rhine, and precipitation on the plain (Pinault & Schomburgk, 2006; Thierion et al., 2012). Based on the observed correlation between dt/t and water table elevation

(Figure 1d), it suggests a potential connection between field observations of seismic velocity variations and environmental changes like rainfalls and basin catchment features in the region. It highlights the potential application of ANI on monitoring environmental factors, which will be a focus of future research.

Changes in ANI measurements resulting from seasonal natural phenomena such as atmospheric pressure loading, can critically be of similar amplitude to those resulting from internal processes of reservoir engineering such as pumping or injection of fluids and induce potential bias in their monitoring. The identification of the driving mechanisms at the origin of reproducible fluctuations in long time-series open new perspectives for the removal of undesirable effects not only in the context of monitoring of geothermal reservoir but also of the evolution of landslides, volcanoes, fault zones, seasonal changes of the crust and so on which are based on ANI measurements. Indeed, studies aimed to correct the time-series from seasonal effects such as those produced by rainfalls and thermoelastic strain (Civilini et al., 2020; Lecocq et al., 2017; Wang et al., 2017) have recently been published.

5. Conclusions

We proposed a novel numerical model to interpret seasonal effects in ambient seismic noise measurements that are typically well documented but insufficiently explained from a physical model. The specificity of our approach relies on the propagation of a diffuse scattered wavefield in a deformable medium taking into account non-linear effects as acousto-elastic effects. We show that our model can explain the temporal evolution of velocity fluctuations measured from noise correlations as being due to small seasonal variations in pressure (of a few kPa) induced by fluctuations of water table elevation. It evidences the high sensitivity of the scattered waves to small strain perturbations in the medium and proposes a clear physical interpretation of this seismic signal.

Data Availability Statement

For the use of SPEC-FEM2D (v7.0.0), a free software downloadable at <https://github.com/geodynamics/spec-fem2d.git>, we thank the Computational Infrastructure for Geodynamics (<http://geodynamics.org>) which is funded by the National Science Foundation under awards EAR-0949446 and EAR-1550901. For the use of Code_ASTER, which is also a free software downloadable at <https://www.code-aster.org/V2/spip.php?rubrique7> (Electricité de France, 1989–2024), we thank Electricité de France (EDF). For the use of water table elevation data, we thank APRONA which is an organization in charge of managing regional groundwater quality observation networks in Alsace, making information freely available on their portal at <https://www.aprona.net>. Direct access to data from station 01995X0103/338B1 can be obtained at the following address: <https://carto.aprona.net/aprona/piezometre/6/>.

Acknowledgments

We thank M. Lehujeur and D. Kula for their technical support to get ambient noise measurements at BETS and RITT stations and to compute related ANCCFs. L. Boschi, L. Alexander, F. Masson are acknowledged for fruitful comments and discussions. We thank D. Sun and two anonymous reviewers for their very helpful comments, which significantly improved the manuscript. Y. Wang was supported by China Scholarship Council (CSC). This work has been performed under the framework of the LABEX ANR-11-LABX-0050-G-EAU-THERMIE-PROFONDE and the Interdisciplinary Thematic Institute GeoT, as part of the ITI 2021–2028 program of the University of Strasbourg, CNRS and Inserm. It was supported by IdEx Unistra (ANR-10-IDEX-0002), and by SFRI-STRAT'US project (ANR-20-SFRI-0012) under the framework of the French Investments for the Future Program. It has also been funded by the EGS Alsace grant from ADEME, the consortium COGEOS (Electricité de Strasbourg/EOST) and a Grant from Storengy/Engie.

References

- Aoki, Y. (2015). Monitoring temporal changes of seismic properties. *Frontiers in Earth Science*, 3. <https://doi.org/10.3389/feart.2015.00042>
- Azzola, J., Schmittbuhl, J., Zigone, D., Lengliné, O., Masson, F., & Magnenet, V. (2020). Elastic strain effects on wave scattering: Implications for coda wave interferometry (CW1). *Journal of Geophysical Research: Solid Earth*, 125(3), e2019JB018974. <https://doi.org/10.1029/2019JB018974>
- Azzola, J., Schmittbuhl, J., Zigone, D., Magnenet, V., & Masson, F. (2018). Direct modeling of the mechanical strain influence on coda wave interferometry. *Journal of Geophysical Research: Solid Earth*, 123(4), 3160–3177. <https://doi.org/10.1002/2017JB015162>
- Baujard, C., Genter, A., Dalmais, E., Maurer, V., Hehn, R., Rosillette, R., et al. (2017). Hydrothermal characterization of wells GRT-1 and GRT-2 in Rittershoffen, France: Implications on the understanding of natural flow systems in the rhine graben. *Geothermics*, 65, 255–268. <https://doi.org/10.1016/j.geothermics.2016.11.001>
- Brenguier, F., Campillo, M., Hadziioannou, C., Shapiro, N. M., Nadeau, R. M., & Larose, E. (2008). Postseismic relaxation along the san andreas fault at parkfield from continuous seismological observations. *Science*, 321(5895), 1478–1481. <https://doi.org/10.1126/science.1160943>
- Brenguier, F., Clarke, D., Aoki, Y., Shapiro, N. M., Campillo, M., & Ferrazzini, V. (2011). Monitoring volcanoes using seismic noise correlations. *Comptes Rendus Geoscience*, 343(8–9), 633–638. <https://doi.org/10.1016/j.crte.2010.12.010>
- Brenguier, F., Courbis, R., Mordret, A., Campman, X., Boué, P., Chmiel, M., et al. (2020). Noise-based ballistic wave passive seismic monitoring. Part I: Body waves. *Geophysical Journal International*, 221(1), 683–691. <https://doi.org/10.1093/gji/ggz440>
- Campillo, M., & Roux, P. (2015). Crust and lithospheric structure - seismic imaging and monitoring with ambient noise correlations. In G. Schubert (Ed.), *Treatise on geophysics* (2nd ed., Vol. 1, pp. 391–417). Elsevier. <https://doi.org/10.1016/B978-0-444-53802-4.00024-5>
- Civilini, F., Savage, M. K., & Townend, J. (2020). Shear-wave velocity changes induced by earthquakes and rainfall at the Rotokawa and Ngatamariki geothermal fields, Taupō Volcanic Zone, New Zealand. *Geophysical Journal International*, 221(1), 97–114. <https://doi.org/10.1093/gji/ggz547>
- Électricité de, F. (1989–2024). Open source finite element code_aster. Version 12.2. [Software] www.code-aster.org. *Analysis of Structures and Thermomechanics for Studies and Research*.
- Fokker, E., Ruigrok, E., Hawkins, R., & Trampert, J. (2021). Physics-based relationship for pore pressure and vertical stress monitoring using seismic velocity variations. *Remote Sensing*, 13(14), 2684. <https://doi.org/10.3390/rs13142684>

- Fokker, E., Ruigrok, E., Hawkins, R., & Trampert, J. (2023). 4D physics-based pore pressure monitoring using passive image interferometry. *Geophysical Research Letters*, *50*(5), e2022GL101254. <https://doi.org/10.1029/2022GL101254>
- Gaubert-Bastide, T., Garambois, S., Bordes, C., Voisin, C., Oxarango, L., Brito, D., & Roux, P. (2022). High-resolution monitoring of controlled water table variations from dense seismic-noise acquisitions. *Water Resources Research*, *58*(8), e2021WR030680. <https://doi.org/10.1029/2021WR030680>
- Hillers, G., & Ben-Zion, Y. (2011). Seasonal variations of observed noise amplitudes at 2-18 Hz in southern California: Seasonal variations of high-f seismic noise. *Geophysical Journal International*, *184*(2), 860–868. <https://doi.org/10.1111/j.1365-246X.2010.04886.x>
- Hillers, G., Ben-Zion, Y., Campillo, M., & Zigone, D. (2015). Seasonal variations of seismic velocities in the San Jacinto fault area observed with ambient seismic noise. *Geophysical Journal International*, *202*(2), 920–932. <https://doi.org/10.1093/gji/ggv151>
- Hughes, D. S., & Kelly, J. L. (1953). Second-order elastic deformation of solids. *Physical Review*, *92*(5), 1145–1149. <https://doi.org/10.1103/PhysRev.92.1145>
- Lecoq, T., Longuevergne, L., Pedersen, H. A., Brenguier, F., & Stammer, K. (2017). Monitoring ground water storage at mesoscale using seismic noise: 30 years of continuous observation and thermo-elastic and hydrological modeling. *Scientific Reports*, *7*(1), 14241. <https://doi.org/10.1038/s41598-017-14468-9>
- Lehujeur, M., Vergne, J., Maggi, A., & Schmittbuhl, J. (2017). Ambient noise tomography with non-uniform noise sources and low aperture networks: Case study of deep geothermal reservoirs in northern Alsace, France. *Geophysical Journal International*, *208*(1), 193–210. <https://doi.org/10.1093/gji/ggw373>
- Lehujeur, M., Vergne, J., Schmittbuhl, J., & Maggi, A. (2015). Characterization of ambient seismic noise near a deep geothermal reservoir and implications for interferometric methods: A case study in northern Alsace, France. *Geothermal Energy*, *3*(3), 3. <https://doi.org/10.1186/s40517-014-0020-2>
- Lengliné, O., Boubacar, M., & Schmittbuhl, J. (2017). Seismicity related to the hydraulic stimulation of GRT1, Rittershoffen, France. *Geophysical Journal International*, *208*(3), ggw490. <https://doi.org/10.1093/gji/ggw490>
- Liu, C., Aslam, K., & Daub, E. (2020). Seismic velocity changes caused by water table fluctuation in the New Madrid seismic zone and Mississippi embayment. *Journal of Geophysical Research: Solid Earth*, *125*(8), e2020JB019524. <https://doi.org/10.1029/2020JB019524>
- Luo, Y. H., Yang, Y. J., Xu, Y. X., Xu, H. R., Zhao, K. F., & Wang, K. (2015). On the limitations of interstation distances in ambient noise tomography. *Geophysical Journal International*, *201*(2), 652–661. <https://doi.org/10.1093/gji/ggv043>
- Mainsant, G., Larose, E., Brönnimann, C., Jongmans, D., Michoud, C., & Jaboyedoff, M. (2012). Ambient seismic noise monitoring of a clay landslide: Toward failure prediction. *Journal of Geophysical Research*, *117*(F1), F01030. <https://doi.org/10.1029/2011JF002159>
- Maurer, V., Gaucher, E., Grunberg, M., Koepke, R., Pestourie, R., & Cuenot, N. (2020). Seismicity induced during the development of the Rittershoffen geothermal field, France. *Geothermal Energy*, *8*, 1–31. <https://doi.org/10.1186/s40517-020-0155-2>
- Mordret, A., Courbis, R., Brenguier, F., Chmiel, M., Garambois, S., Mao, S., et al. (2020). Noise-based ballistic wave passive seismic monitoring – Part 2: Surface waves. *Geophysical Journal International*, *221*(1), 692–705. <https://doi.org/10.1093/gji/ggaa016>
- Mordret, A., Mikesell, T. D., Harig, C., Lipovsky, B. P., & Prieto, G. A. (2016). Monitoring southwest Greenland's ice sheet melt with ambient seismic noise. *Science Advances*, *2*(5), e1501538. <https://doi.org/10.1126/sciadv.1501538>
- Nakata, N., Gualtieri, L., & Fichtner, A. (Eds.) (2019). In *Seismic ambient noise*. Cambridge University Press.
- Obermann, A., Froment, B., Campillo, M., Larose, E., Planès, T., Valette, B., et al. (2014). Seismic noise correlations to image structural and mechanical changes associated with the M_w 7.9 2008 Wenchuan earthquake. *Journal of Geophysical Research: Solid Earth*, *119*(4), 3155–3168. <https://doi.org/10.1002/2013JB010932>
- Obermann, A., Kraft, T., Larose, E., & Wiemer, S. (2015). Potential of ambient seismic noise techniques to monitor the St. Gallen geothermal site (Switzerland). *Journal of Geophysical Research: Solid Earth*, *120*(6), 4301–4316. <https://doi.org/10.1002/2014JB011817>
- Olivier, G., Brenguier, F., Campillo, M., Lynch, R., & Roux, P. (2015). Body-wave reconstruction from ambient seismic noise correlations in an underground mine. *Geophysics*, *80*(3), KS11–KS25. <https://doi.org/10.1190/geo2014-0299.1>
- Paul, A., Campillo, M., Margerin, L., Larose, E., & Derode, A. (2005). Empirical synthesis of time-asymmetrical Green functions from the correlation of coda waves. *Journal of Geophysical Research*, *110*(B8), B08302. <https://doi.org/10.1029/2004JB003521>
- Pinault, J. L., & Schomburgk, S. (2006). Inverse modeling for characterizing surface water/groundwater exchanges. *Water Resources Research*, *42*(8), W08414. <https://doi.org/10.1029/2005WR004587>
- Pride, S. R., Berryman, J. G., & Harris, J. M. (2004). Seismic attenuation due to wave-induced flow. *Journal of Geophysical Research*, *109*(B1). <https://doi.org/10.1029/2003JB002639>
- Sabra, K. G., Gerstoft, P., Roux, P., Kuperman, W. A., & Fehler, M. C. (2005). Extracting time-domain Green's function estimates from ambient seismic noise. *Geophysical Research Letters*, *32*(3), L03310. <https://doi.org/10.1029/2004GL021862>
- Sánchez-Pastor, P., Obermann, A., Schimmel, M., Weemstra, C., Verdel, A., & Jousset, P. (2019). Short- and long-term variations in the reykjanes geothermal reservoir from seismic noise interferometry. *Geophysical Research Letters*, *46*(11), 5788–5798. <https://doi.org/10.1029/2019GL082352>
- Sens-schönfelder, C., Pomponi, E., & Peltier, A. (2014). Dynamics of Piton de la Fournaise volcano observed by passive image interferometry with multiple references. *Journal of Volcanology and Geothermal Research*, *276*, 32–45. <https://doi.org/10.1016/j.jvolgeores.2014.02.012>
- Sens-Schönfelder, C., & Wegler, U. (2006). Passive image interferometry and seasonal variations of seismic velocities at Merapi Volcano, Indonesia. *Geophysical Research Letters*, *33*(21), L21302. <https://doi.org/10.1029/2006GL027797>
- Silver, P. G., Daley, T. M., Niu, F., & Majer, E. L. (2007). Active source monitoring of cross-well seismic travel time for stress-induced changes. *Bulletin of the Seismological Society of America*, *97*(1B), 281–293. <https://doi.org/10.1785/0120060120>
- Smith, R. T. (1963). Stress-induced anisotropy in solids—The acousto-elastic effect. *Ultrasonics*, *1*(3), 135–147. [https://doi.org/10.1016/0041-624X\(63\)90003-9](https://doi.org/10.1016/0041-624X(63)90003-9)
- Snieder, R. (2006). The theory of coda wave interferometry. *Pure and Applied Geophysics*, *163*(2-3), 455–473. <https://doi.org/10.1007/s00024-005-0026-6>
- Stacey, R. (1988). Improved transparent boundary formulations for the elastic-wave equation. *Bulletin of the Seismological Society of America*, *78*(6), 2089–2097. <https://doi.org/10.1785/BSSA0780062089>
- Thierion, C., Longuevergne, L., Habets, F., Ledoux, E., Ackerer, P., Majdalani, S., et al. (2012). Assessing the water balance of the upper rhine graben hydrosystem. *Journal of Hydrology*, *424*, 68–83. <https://doi.org/10.1016/j.jhydrol.2011.12.028>
- Toupin, R. A., & Bernstein, B. (1961). Sound waves in deformed perfectly elastic materials. Acoustoelastic effect. *Journal of the Acoustical Society of America*, *33*(2), 216–225. <https://doi.org/10.1121/1.1908623>
- Tsai, V. C. (2011). A model for seasonal changes in GPS positions and seismic wave speeds due to thermoelastic and hydrologic variations. *Journal of Geophysical Research*, *116*(B4), B04404. <https://doi.org/10.1029/2010JB008156>

- Vallier, B., Magnenet, V., Schmittbuhl, J., & Fond, C. (2018). THM modeling of hydrothermal circulation at Rittershoffen geothermal site, France. *Geothermal Energy*, 6(1), 22. <https://doi.org/10.1186/s40517-018-0108-1>
- Vallier, B., Magnenet, V., Schmittbuhl, J., & Fond, C. (2019). Large scale hydro-thermal circulation in the deep geothermal reservoir of Soultz-sous-Forêts (France). *Geothermics*, 78, 154–169. <https://doi.org/10.1016/j.geothermics.2018.12.002>
- Voisin, C., Garambois, S., Massey, C., & Brossier, R. (2016). Seismic noise monitoring of the water table in a deep-seated, slow-moving landslide. *Interpretation*, 4(3), SJ67–SJ76. <https://doi.org/10.1190/INT-2016-0010.1>
- Wang, Q.-Y., Brenguier, F., Campillo, M., Lecointre, A., Takeda, T., & Aoki, Y. (2017). Seasonal crustal seismic velocity changes throughout Japan. *Journal of Geophysical Research: Solid Earth*, 122(10), 7987–8002. <https://doi.org/10.1002/2017JB014307>
- Wang, Q. Y., & Yao, H. (2020). Monitoring of velocity changes based on seismic ambient noise: A brief review and perspective. *Earth and Planetary Physics*, 4(5), 532–542. <https://doi.org/10.26464/epp2020048>
- Wegler, U., & Lühr, B. G. (2001). Scattering behaviour at Merapi volcano (Java) revealed from an active seismic experiment. *Geophysical Journal International*, 145(3), 579–592. <https://doi.org/10.1046/j.1365-246x.2001.01390.x>
- Winkler, K. W., & Liu, X. (1996). Measurements of third-order elastic constants in rocks. *Journal of the Acoustical Society of America*, 100(3), 1392–1398. <https://doi.org/10.1121/1.415986>
- Yamamura, K., Sano, O., Utada, H., Takei, Y., Nakao, S., & Fukao, Y. (2003). Long-term observation of in situ seismic velocity and attenuation. *Journal of Geophysical Research*, 108(B6), 2317. <https://doi.org/10.1029/2002JB002005>
- Yates, A. S., Savage, M. K., Jolly, A. D., Caudron, C., & Hamling, I. J. (2019). Volcanic, coseismic, and seasonal changes detected at White Island (Whakaari) Volcano, New Zealand, using seismic ambient noise. *Geophysical Research Letters*, 46(1), 99–108. <https://doi.org/10.1029/2018GL080580>
- Zhan, Z., Tsai, V., & Clayton, R. W. (2013). Spurious velocity changes caused by temporal variations in ambient noise frequency content. *Geophysical Journal International*, 194(3), 1574–1581. <https://doi.org/10.1093/gji/ggt170>